A State-Independent Linear Power Flow Model With Accurate Estimation of Voltage Magnitude

Jingwei Yang, *Student Member, IEEE*, Ning Zhang, *Member, IEEE*, Chongqing Kang, *Fellow, IEEE*, and Qing Xia, *Senior Member, IEEE*

***Abstract*—Linearized power flow models are of great interest in power system studies such as contingency analyses and reliability assessments, especially for large-scale systems. One of the most popular models—the classical DC power flow model—is widely used and praised for its state independence, robustness, and computational efficiency. Despite its advantages, however, the DC power flow model fails to consider reactive power or bus voltage magnitude. This paper closes this gap by proposing a decoupled linearized power flow (DLPF) model with respect to voltage magnitude and phase angle. The model is state independent but is distinguished by its high accuracy in voltage magnitude. Moreover, this paper presents an in-depth analysis of the DLPF model with the purpose of accelerating its computation speed, leading to the fast DLPF (FDLPF) model. The approximation that is applied to obtain the FDLPF model from the DLPF model is justified by a theoretical derivation and numerical tests. The proposed methods are provably accurate and robust for several cases, including radial distribution systems, meshed large-scale transmission systems and ill-conditioned systems. Finally, expressions for sensitivity with regard to MW flow and bus voltage are provided as a potential application.**

***Index Terms*—Computational efficiency, decoupled load flow, linear power flow model, optimal power flow, reactive power, voltage magnitude.**

NOMENCLATURE

The main notation used in this paper is provided below; other symbols are defined as required.

n	Number of power system buses
m	Number of power system lines
$\mathcal{R}$	Set of $V\theta$ buses (slack buses)
$\mathcal{S}$	Set of PV buses
$\mathcal{L}$	Set of PQ buses
$\boldsymbol{Y} = \boldsymbol{G} + j\boldsymbol{B}$	Admittance matrix of the power system
$\boldsymbol{Y'} = \boldsymbol{G'} + j\boldsymbol{B'}$	Admittance matrix without shunt elements
$Y_{ij} = G_{ij} + jB_{ij}$	Element in the ith row and jth column of $\boldsymbol{Y}$
$Y'_{ij} = G'_{ij} + jB'_{ij}$	Element in the ith row and jth column of $\boldsymbol{Y'}$
$\boldsymbol{V}, \boldsymbol{\theta}$	Magnitudes and phase angles of bus voltages
V_i, θ_i	Voltage magnitude and phase angle of bus i
$\boldsymbol{P}, \boldsymbol{Q}$	Bus injected active and reactive powers
P_i, Q_i	Injected active and reactive power at bus i
P_{ij}	Lossless MW flow from bus i to bus j
$z_{ij} = r_{ij} + jx_{ij}$	Impedance of line (i, j)
$y_{ij} = g_{ij} + jb_{ij}$	Admittance of line (i, j)
$y_{ii} = g_{ii} + jb_{ii}$	Shunt admittance at bus i

Manuscript received March 10, 2016; revised June 24, 2016, September 1, 2016, and October 30, 2016; accepted December 10, 2016. Date of publication December 13, 2016; date of current version August 17, 2017. This work was supported in part by the National Key Research and Development Program of China (No. 2016YFB0900102), the National Science Fund Major International (Regional) Joint Research Project of China (No. 51620105007), and the Tsinghua University Initiative Scientific Research Program (No. 20151080418). Paper no. TPWRS-00380-2016. *(Corresponding author: Chongqing Kang.)*

The authors are with the State Key Laboratory of Power Systems, Department of Electrical Engineering, Tsinghua University, Beijing 100084, China (e-mail: cqkang@tsinghua.edu.cn).

Color versions of one or more of the figures in this paper are available online at http://ieeexplore.ieee.org.

Digital Object Identifier 10.1109/TPWRS.2016.2638923

I. INTRODUCTION

POWER flow analysis is the backbone of power system studies and is widely applied in daily operations as well as short-term and long-term planning. Direct calculations of power flow are of great significance for contingency analysis [1], reliability assessment [2] and probabilistic load flow analysis [3], if they can be performed accurately and efficiently. Although conventional AC power flow calculations yield accurate results, their nonlinearity, difficulty in convergence and low computational efficiency limit their application in the power system industry, especially for large-scale systems [4]. Therefore, a fast and linear power flow model would be of great interest, provided it could offer reasonable accuracy and robustness for all types of grids. Such a linear model could also be beneficial for solving optimization problems [5], such as locational marginal pricing (LMP) and security-constrained unit commitment (SCUC), by allowing these problems to be transformed into linear programming problems [6].

The DC power flow model is one of the most widely used linear power flow models for power systems. Because it is a linear, non-iterative model with reasonable accuracy in terms of MW flow, it has considerable analytical and computational appeal compared with the AC power flow model [7]. The classical DC power flow model is derived based on the assumptions of a lossless MW flow and a flat bus voltage profile. More general versions of the DC power flow model have been proposed, including hot- and cold-start models, for broader applications. Hot-start models correct the bus power injections according to base points obtained from initial AC power flow solutions in

various ways, such as net loss dispersal and base-point matching [7]. However, in situations such as DC-model-based SCUC [6], financial transmission rights allocations [8] and power system planning, no reliable AC base points are available. Therefore, it is necessary to use cold-start models. As alternatives to the classical DC power flow model, some cold-start models modify the bus injections by estimating loss as a percentage of net load, whereas others apply an empirical fixed voltage magnitude. Several tests have shown, however, that there is no large difference in MW-flow error between the classical DC power flow model and other cold-start models [7].

Although cold-start DC power flow models are widely used in many fields, it is worth noting that they can neither consider reactive power nor shed light on bus voltage magnitude. In fact, the lack of a voltage magnitude consideration leads to many problems in system planning and operation when cold-start DC power flow models are applied. For instance, it is a common practice to simply consider the MW flows in reliability evaluations. The bus voltage quality is inevitably ignored, and moreover, ZIP loads are modeled at nominal and typical voltages [2]. In terms of electricity markets, only active generation is priced in markets such as PJM. The reactive power offered by generators is paid for merely as an ancillary service [9]. Probabilistic load flow calculations, which are an increasingly important tool in power system analysis, typically face the dilemma that DC power flow models are incapable of accounting for voltage magnitude, whereas AC power flow models that are linearized around the operating point lead to errors in scenarios with large signal perturbations [10].

However, it is not easy to consider bus voltage magnitudes in a decoupled linear flow model, because they are sensitive to both active and reactive power injections. In [11], a linear model was proposed for radial distribution systems. However, this model is dependent on the radial topology of the distribution system and cannot be extended to meshed transmission systems. The authors of [12] have achieved a great advancement in formulating a linear load equation that considers reactive power. This power flow model reflects both active and reactive power balance with respect to the square of the voltage magnitude, V^2, and the modified phase angle, $V^2\theta$. Nevertheless, the voltage magnitude and phase angle are not completely decoupled, giving rise to a quadratic programming problem if this model is applied for optimization.

This paper makes a further step toward a $V-\theta$ decoupled linear power flow model, which is distinguished by its accuracy in voltage magnitude and robustness for various types of systems. Moreover, we direct considerable attention to improving its computational efficiency for potential application to large-scale systems or simulations that require tens of millions of repeated load flow calculations. The specific contributions of this paper are threefold:

1) To propose a decoupled linearized power flow (DLPF) model with respect to the voltage magnitude V and the phase angle θ. The model is distinguished by its accuracy in voltage magnitude and robustness for application to different types of systems. The error in MW flow is comparable to that of cold-start DC power flow models, which is much smaller in practice than is predicted, as mentioned in [7].
2) To design a fast DLPF (FDLPF) model by developing a fast approximation of the matrices used in the DLPF model, which is as fast as classical DC power flow calculations while still as accurate as DLPF calculations. The approximation is justified by a theoretical derivation and numerical tests.
3) To provide linear expressions for sensitivity computations regarding MW flow and bus voltage magnitude. The sensitivity is much greater than a small-signal sensitivity. Numerical results prove that the model can also be applied in cases of large signal perturbations.

The remainder of the paper is organized as follows. Section II formulates the DLPF model based on the initial AC power flow equation and derives the expressions for voltage magnitude, phase angle and branch MW flow. In Section III, the FDLPF model is formulated by making a subtle change to the DLPF model, which is justified by a theoretical derivation and numerical examples. The specific steps for utilizing the FDLPF model are presented in order in Section IV. In Section V, several cases, including radial distribution systems, meshed large-scale transmission systems and ill-conditioned systems, are analyzed to demonstrate the accuracy and robustness of the DLPF/FDLPF approach and the computational efficiency of the FDLPF model. Large-signal sensitivity expressions are provided in Section VI as an application of the FDLPF model. Finally, conclusions are drawn and further discussions are presented.

II. Formulation and Derivation of the DLPF

A. Decoupling of Voltage Magnitude and Phase Angle

For a power system with n buses, the polar power-voltage AC power flow model is well known:

$$P_i = \sum_{j=1}^{n} G_{ij}V_iV_j\cos\theta_{ij} + \sum_{j=1}^{n} B_{ij}V_iV_j\sin\theta_{ij} \tag{1}$$

$$Q_i = -\sum_{j=1}^{n} B_{ij}V_iV_j\cos\theta_{ij} + \sum_{j=1}^{n} G_{ij}V_iV_j\sin\theta_{ij} \tag{2}$$

$$i = 1, 2, \cdots, n$$

For most scenarios in real power systems, the bus voltage magnitudes are approximately 1 p.u. The absolute value of phase angle differences across lines rarely exceed 30° [12] and most of them are within 10° [13]. Moreover, the admittance matrix of the power system has a special structure, in which the diagonal elements are the sum of the non-diagonal elements in the corresponding rows, with the contribution of shunt elements as well:

$$Y_{ij} = \begin{cases} -y_{ij} & \text{if } j \neq i \\ y_{ii} + \sum_{k=1,k\neq i}^{n} y_{ik} & \text{if } j = i \end{cases} \tag{3}$$

Note that in this paper, the "shunt elements" y_{ii} denote not only the contribution of shunt capacitors but also the line-charging susceptance and the equivalent admittance of transformers and

phase shifters (Part C of this section provides the details of the consideration of transformers and phase shifters).

Considering these facts, the following linear approximations are applied to (1) to decouple the voltage magnitudes and the phase angles:

$$\begin{aligned} P_i &= \sum_{j=1}^{n} G_{ij}V_iV_j\cos\theta_{ij} + \sum_{j=1}^{n} B_{ij}V_iV_j\sin\theta_{ij} \\ &= g_{ii}V_i^2 + \sum_{j=1,j\neq i}^{n} \left(g_{ij}V_i\left(V_i - V_j\cos\theta_{ij}\right)\right. \\ &\quad \left. - b_{ij}V_iV_j\sin\theta_{ij}\right) \\ &\approx g_{ii}V_i + \sum_{j=1,j\neq i}^{n} g_{ij}\left(V_i - V_j\right) - \sum_{j=1,j\neq i}^{n} b_{ij}\left(\theta_i - \theta_j\right) \\ &= \left(V_i\sum_{j=1}^{n} g_{ij} + \sum_{j=1,j\neq i}^{n}\left(-g_{ij}\right)V_j\right) \\ &\quad - \left(\theta_i\sum_{j=1,j\neq i}^{n} b_{ij} + \sum_{j=1,j\neq i}^{n}\left(-b_{ij}\right)\theta_j\right) \\ &= \sum_{j=1}^{n} G_{ij}V_j - \sum_{j=1}^{n} B'_{ij}\theta_j \end{aligned} \tag{4}$$

Similarly, equation (2) for reactive power can be approximated as follows:

$$Q_i = -\sum_{j=1}^{n} B_{ij}V_j - \sum_{j=1}^{n} G_{ij}\theta_j \tag{5}$$

Note that $G'_{ij} \approx G_{ij}$ is assumed in (5) because the shunt conductance is negligible compared with the shunt susceptance.

The approximations made in (4) and (5) are not the same as those made in other linear power flow models. Consider the following three alternative approximations in the expression of branch MW flow, corresponding to the DC power flow, the approximation made by [12], and the proposed approximation, respectively:

1) Approx.1: $g_{ij}V_i(V_i - V_j\cos\theta_{ij}) \approx 0$
2) Approx.2: $g_{ij}V_i(V_i - V_j\cos\theta_{ij}) \approx g_{ij}\left(V_i^2 - V_j^2\right)$
3) Approx.3: $g_{ij}V_i(V_i - V_j\cos\theta_{ij}) \approx g_{ij}\left(V_i - V_j\right)$

The common assumption is that $\cos\theta_{ij} \approx 1$. However, the methods dealing with voltage magnitude are not identical. In the DC model, the voltage differences across branches are neglected. However, these are considered in Approx.3, which is the key approximation step in the derivation of the proposed DLPF model. Although [12] takes voltage differences into account by using Approx.2, the result is not satisfactory. Fig. 1 illustrates the effects of the three approximations on branch MW flow in two typical scenarios (a high r/x ratio and a low r/x ratio). It is evident that the approximation proposed in this paper (Approx. 3) performs the best in both cases.

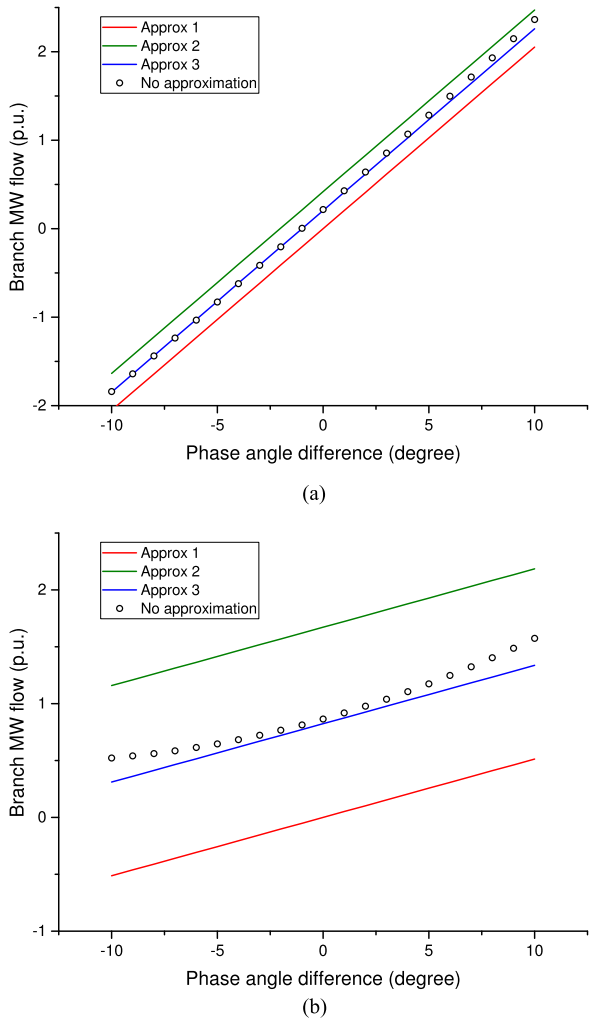

Fig. 1. An illustration of the accuracy of different approximations with $V_i = 1.05$ p.u. and $V_j = 0.98$ p.u.

In fact, a theoretical mechanism exists underlying the proposed approximation:

$$\begin{aligned} g_{ij}V_i(V_i - V_j\cos\theta_{ij}) &\approx g_{ij}V_i\left(V_i - V_j\right) \\ &= g_{ij}\left(1 + \Delta V_i\right)\left(\Delta V_i - \Delta V_j\right) \\ &\approx g_{ij}\left(\Delta V_i - \Delta V_j\right) \\ &= g_{ij}\left(1 + \Delta V_i - 1 - \Delta V_j\right) \\ &= g_{ij}\left(V_i - V_j\right) \end{aligned} \tag{6}$$

Note that V_i is decomposed into $(1 + \Delta V_i)$, where ΔV_i is typically one order of magnitude smaller than V_i. In the second step of (6), ΔV_i^2 and $\Delta V_i \Delta V_j$ can be neglected without excessive error because they are two orders of magnitude smaller than V_i and V_j.

A linear expression for the average branch MW flow P_{ij} can also be easily obtained from the first step of (4):

$$P_{ij} = g_{ij}\left(V_i - V_j\right) - b_{ij}\left(\theta_i - \theta_j\right) \tag{7}$$

Because the line loss is ignored for linearity, we have $P_{ij} = -P_{ji}$, where P_{ij} denotes the power flow from bus i to bus

j. It should be noted that equation (7) has to be modified for lines with transformers and phase shifters. The details are also provided in Part C.

B. Matrix Formulation of the DLPF Model

Equations (4) and (5) represent the basic formulation of the DLPF model. The matrix form is as follows:

$$\begin{bmatrix} \boldsymbol{P} \\ \boldsymbol{Q} \end{bmatrix} = - \begin{bmatrix} \boldsymbol{B}' & -\boldsymbol{G} \\ \boldsymbol{G} & \boldsymbol{B} \end{bmatrix} \begin{bmatrix} \boldsymbol{\theta} \\ \boldsymbol{V} \end{bmatrix} \tag{8}$$

It is evident that both $\boldsymbol{\theta}$ and $\boldsymbol{V}$ consist of three sub-vectors, corresponding to the $V\theta$, PV, and PQ buses. Without loss of generality, we arrange these buses in the following sequence: $V\theta$, PV, PQ.

$$\begin{aligned} \boldsymbol{\theta} &= \begin{bmatrix} \boldsymbol{\theta}_{\mathcal{R}}^T, & \boldsymbol{\theta}_{\mathcal{S}}^T, & \boldsymbol{\theta}_{\mathcal{L}}^T \end{bmatrix}^T \\ \boldsymbol{V} &= \begin{bmatrix} \boldsymbol{V}_{\mathcal{R}}^T, & \boldsymbol{V}_{\mathcal{S}}^T, & \boldsymbol{V}_{\mathcal{L}}^T \end{bmatrix}^T \end{aligned} \tag{9}$$

The admittance matrix $\boldsymbol{Y}$ can also be partitioned in the same manner:

$$\boldsymbol{Y} = \begin{bmatrix} \boldsymbol{Y}_{\mathcal{RR}} & \boldsymbol{Y}_{\mathcal{RS}} & \boldsymbol{Y}_{\mathcal{RL}} \\ \boldsymbol{Y}_{\mathcal{SR}} & \boldsymbol{Y}_{\mathcal{SS}} & \boldsymbol{Y}_{\mathcal{SL}} \\ \boldsymbol{Y}_{\mathcal{LR}} & \boldsymbol{Y}_{\mathcal{LS}} & \boldsymbol{Y}_{\mathcal{LL}} \end{bmatrix} \tag{10}$$

With the aid of the known sub-vectors $\boldsymbol{\theta}_{\mathcal{R}}$, $\boldsymbol{V}_{\mathcal{R}}$, and $\boldsymbol{V}_{\mathcal{S}}$, we transform (8) into the following equation:

$$\begin{bmatrix} \tilde{\boldsymbol{P}} \\ \tilde{\boldsymbol{Q}} \end{bmatrix} = \begin{bmatrix} \boldsymbol{H} & \boldsymbol{N} \\ \boldsymbol{M} & \boldsymbol{L} \end{bmatrix} \begin{bmatrix} \tilde{\boldsymbol{\theta}} \\ \tilde{\boldsymbol{V}} \end{bmatrix} \tag{11}$$

where

$$\begin{bmatrix} \tilde{\boldsymbol{P}} \\ \tilde{\boldsymbol{Q}} \end{bmatrix} = \begin{bmatrix} \boldsymbol{P}_{\mathcal{S}} \\ \boldsymbol{P}_{\mathcal{L}} \\ \boldsymbol{Q}_{\mathcal{L}} \end{bmatrix} + \begin{bmatrix} \boldsymbol{B}'_{\mathcal{SR}} & -\boldsymbol{G}_{\mathcal{SR}} & -\boldsymbol{G}_{\mathcal{SS}} \\ \boldsymbol{B}'_{\mathcal{LR}} & -\boldsymbol{G}_{\mathcal{LR}} & -\boldsymbol{G}_{\mathcal{LS}} \\ \boldsymbol{G}_{\mathcal{LR}} & \boldsymbol{B}_{\mathcal{LR}} & \boldsymbol{B}_{\mathcal{LS}} \end{bmatrix} \begin{bmatrix} \boldsymbol{\theta}_{\mathcal{R}} \\ \boldsymbol{V}_{\mathcal{R}} \\ \boldsymbol{V}_{\mathcal{S}} \end{bmatrix} \tag{12}$$

$$\begin{bmatrix} \boldsymbol{H} & \boldsymbol{N} \\ \boldsymbol{M} & \boldsymbol{L} \end{bmatrix} = - \left[\begin{array}{cc|c} \boldsymbol{B}'_{\mathcal{SS}} & \boldsymbol{B}'_{\mathcal{SL}} & -\boldsymbol{G}_{\mathcal{SL}} \\ \boldsymbol{B}'_{\mathcal{LS}} & \boldsymbol{B}'_{\mathcal{LL}} & -\boldsymbol{G}_{\mathcal{LL}} \\ \hline \boldsymbol{G}_{\mathcal{LS}} & \boldsymbol{G}_{\mathcal{LL}} & \boldsymbol{B}_{\mathcal{LL}} \end{array}\right] \tag{13}$$

$$\begin{aligned} \tilde{\boldsymbol{\theta}} &= \begin{bmatrix} \boldsymbol{\theta}_{\mathcal{S}}^T, \boldsymbol{\theta}_{\mathcal{L}}^T & \end{bmatrix}^T \\ \tilde{\boldsymbol{V}} &= \boldsymbol{V}_{\mathcal{L}} \end{aligned} \tag{14}$$

Performing elementary row operations on both sides of (11) leads to the following equations:

$$\begin{bmatrix} \tilde{\boldsymbol{P}} - \boldsymbol{N}\boldsymbol{L}^{-1}\tilde{\boldsymbol{Q}} \\ \tilde{\boldsymbol{Q}} \end{bmatrix} = \begin{bmatrix} \boldsymbol{H} - \boldsymbol{N}\boldsymbol{L}^{-1}\boldsymbol{M} & \boldsymbol{0} \\ \boldsymbol{M} & \boldsymbol{L} \end{bmatrix} \begin{bmatrix} \tilde{\boldsymbol{\theta}} \\ \tilde{\boldsymbol{V}} \end{bmatrix} \tag{15}$$

and

$$\begin{bmatrix} \tilde{\boldsymbol{P}} \\ \tilde{\boldsymbol{Q}} - \boldsymbol{M}\boldsymbol{H}^{-1}\tilde{\boldsymbol{P}} \end{bmatrix} = \begin{bmatrix} \boldsymbol{H} & \boldsymbol{N} \\ \boldsymbol{0} & \boldsymbol{L} - \boldsymbol{M}\boldsymbol{H}^{-1}\boldsymbol{N} \end{bmatrix} \begin{bmatrix} \tilde{\boldsymbol{\theta}} \\ \tilde{\boldsymbol{V}} \end{bmatrix} \tag{16}$$

Combining the first part of (15) and the second part of (16) into one equation leads to the decoupling of voltage magnitudes and phase angles:

$$\begin{bmatrix} \tilde{\boldsymbol{P}} - \boldsymbol{N}\boldsymbol{L}^{-1}\tilde{\boldsymbol{Q}} \\ \tilde{\boldsymbol{Q}} - \boldsymbol{M}\boldsymbol{H}^{-1}\tilde{\boldsymbol{P}} \end{bmatrix} = \begin{bmatrix} \tilde{\boldsymbol{H}} & \boldsymbol{0} \\ \boldsymbol{0} & \tilde{\boldsymbol{L}} \end{bmatrix} \begin{bmatrix} \tilde{\boldsymbol{\theta}} \\ \tilde{\boldsymbol{V}} \end{bmatrix} \tag{17}$$

where

$$\tilde{\boldsymbol{H}} = \boldsymbol{H} - \boldsymbol{N}\boldsymbol{L}^{-1}\boldsymbol{M} \tag{18}$$

$$\tilde{\boldsymbol{L}} = \boldsymbol{L} - \boldsymbol{M}\boldsymbol{H}^{-1}\boldsymbol{N} \tag{19}$$

According to (17), the expressions for calculating the unknown $\tilde{\boldsymbol{V}}$ and $\tilde{\boldsymbol{\theta}}$ with respect to the known bus injections $\tilde{\boldsymbol{P}}$ and $\tilde{\boldsymbol{Q}}$ are as follows:

$$\tilde{\boldsymbol{\theta}} = \tilde{\boldsymbol{H}}^{-1}\tilde{\boldsymbol{P}} - \tilde{\boldsymbol{H}}^{-1}\boldsymbol{N}\boldsymbol{L}^{-1}\tilde{\boldsymbol{Q}} \tag{20}$$

$$\tilde{\boldsymbol{V}} = \tilde{\boldsymbol{L}}^{-1}\tilde{\boldsymbol{Q}} - \tilde{\boldsymbol{L}}^{-1}\boldsymbol{M}\boldsymbol{H}^{-1}\tilde{\boldsymbol{P}} \tag{21}$$

Note that the decoupling of the voltage magnitudes and phase angles is not achieved by simply ignoring the relatively small conductance matrix $\boldsymbol{G}$. On the contrary, the coupling between the active and reactive powers is considered in equations (20) and (21).

C. Transformers and Phase Shifters

This section describes the changes to the admittance matrix and MW flow approximations needed for branches with transformers or phase shifters.

1) Contributions to the Admittance Matrix: According to the formation of nodal admittance matrix $\boldsymbol{Y}$ [14], the contribution of the branch with a phase shifting transformer (Fig. 2, t for tap ratio and θ_s for phase shifting angle) to the nodal admittance matrix is

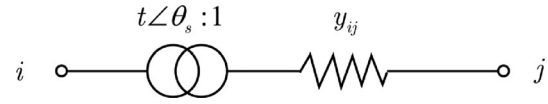

Fig. 2. A general diagram for a branch with phase shifting transformers.

$$\Delta\boldsymbol{Y} = \boldsymbol{C} y_{ij} \overline{\boldsymbol{C}}^T \tag{22}$$

where $\boldsymbol{C}$ is a $n \times 1$ vector of all zeros except $\boldsymbol{C}_i = \frac{1}{te^{-j\theta_s}}$ and $\boldsymbol{C}_j = -1$. $\overline{\boldsymbol{C}}$ is the conjugate of $\boldsymbol{C}$.

$\Delta\boldsymbol{Y}$ can be split into two parts:

$$\Delta\boldsymbol{Y} = \Delta\boldsymbol{Y}_1 + \Delta\boldsymbol{Y}_2 \tag{23}$$

where $\Delta\boldsymbol{Y}_1$ has four non-zero elements:

$$\begin{aligned} \Delta\boldsymbol{Y}_{1,ii} &= -\Delta\boldsymbol{Y}_{1,ij} = \frac{y_{ij}}{te^{-j\theta s}} \\ \Delta\boldsymbol{Y}_{1,jj} &= -\Delta\boldsymbol{Y}_{1,ji} = \frac{y_{ij}}{te^{j\theta s}} \end{aligned} \tag{24}$$

while $\Delta\boldsymbol{Y}_2$ is a diagonal matrix with only two non-zero elements:

$$\begin{aligned} \Delta\boldsymbol{Y}_{2,ii} &= \frac{y_{ij}}{t^2} - \frac{y_{ij}}{te^{-j\theta s}} \\ \Delta\boldsymbol{Y}_{2,jj} &= y_{ij} - \frac{y_{ij}}{te^{j\theta s}} \end{aligned} \tag{25}$$

In fact, $\Delta \boldsymbol{Y}_1$ represents the contribution of equivalent line admittance to $\boldsymbol{Y}$. $\Delta \boldsymbol{Y}_2$ can be regarded as the equivalent shunt elements of phase shifting transformers and is considered in y_{ii} as stated in Part A.

2) Influence on the Branch MW Flow: For the branch shown in Fig. 2, the branch complex power has the following relationship with bus voltage and phase angle:

$$\begin{bmatrix} \overline{S}_{ij} \\ \overline{S}_{ji} \end{bmatrix} = \begin{bmatrix} V_i e^{-j\theta_i} & \\ & V_j e^{-j\theta_j} \end{bmatrix} \begin{bmatrix} \frac{y_{ij}}{t^2} & -\frac{y_{ij}}{te^{-j\theta_s}} \\ -\frac{y_{ij}}{te^{j\theta_s}} & y_{ij} \end{bmatrix} \times \begin{bmatrix} V_i e^{j\theta_i} \\ V_j e^{j\theta_j} \end{bmatrix} \tag{26}$$

The branch MW flow P_{ij} is the real part of $\overline{S}_{ij}$:

$$\begin{aligned} P_{ij} &= \mathrm{Re}\left(V_i e^{-j\theta_i}\left(\frac{y_{ij}}{t^2}V_i e^{j\theta_i} - \frac{y_{ij}}{te^{-j\theta s}}V_j e^{j\theta_j}\right)\right) \\ &= \mathrm{Re}\left(\frac{y_{ij}}{t^2}V_i^2 - \frac{y_{ij}}{t}V_i V_j e^{-j(\theta_i-\theta_j-\theta_s)}\right) \\ &= \frac{g_{ij}}{t}V_i\left(\frac{V_i}{t} - V_i V_j\cos(\theta_i-\theta_j-\theta_s)\right) \\ &\quad - \frac{b_{ij}}{t}V_i V_j \sin(\theta_i-\theta_j-\theta_s) \\ &\approx \frac{g_{ij}}{t}\left(\frac{V_i}{t} - V_j\right) - \frac{b_{ij}}{t}(\theta_i-\theta_j-\theta_s) \end{aligned} \tag{27}$$

The approximation made in the last step of (27) is similar to that in (4) and this provides a linear expression for branch MW flow with transformers or phase shifters. Because the line loss is ignored for linearity, we have $P_{ij} = -P_{ji}$. It should be noted that (27) and (7) have the same pattern. Equation (7) can be seen as a special case of (27) where $t = 1$ and $\theta_s = 0$.

III. Derivation and Justification of the FDLPF

A fast computation speed is one of the key advantages of DC power flow models. The classical DC power flow model achieves this speed because the admittance matrix is formulated using $1/x_{ij}$ directly from the system information. For the DLPF model proposed in Section II, its solution requires the factorization of four matrices: $\boldsymbol{H}$, $\boldsymbol{L}$, $\tilde{\boldsymbol{H}}$, and $\tilde{\boldsymbol{L}}$. Although $\boldsymbol{H}$ and $\boldsymbol{L}$ are sparse matrices, $\tilde{\boldsymbol{H}}$ and $\tilde{\boldsymbol{L}}$ may be non-sparse matrices, for which factorization is computationally intractable. This section, however, shows that $\tilde{\boldsymbol{H}}$ and $\tilde{\boldsymbol{L}}$ can be approximated by the sparse matrices $\tilde{\boldsymbol{H}}'$ and $\tilde{\boldsymbol{L}}'$, which have the same structure as $\boldsymbol{H}$ and $\boldsymbol{L}$:

$$\tilde{H}'_{ij} = \begin{cases} -\dfrac{1}{x_{ij}} & \text{if } j \neq i \\ \sum_{k=1,k\neq i}^{n} \dfrac{1}{x_{ik}} & \text{if } j = i \end{cases} \tag{28}$$

$$\tilde{L}'_{ij} = \begin{cases} -\dfrac{1}{x_{ij}} & \text{if } j \neq i \\ \sum_{k=1}^{n} \dfrac{1}{x_{ik}} & \text{if } j = i \end{cases} \tag{29}$$

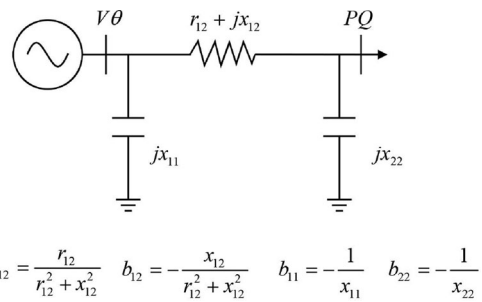

Fig. 3. A 2-bus system.

Expressions (20) and (21) for bus voltage magnitude and phase angle are thus transformed into

$$\tilde{\boldsymbol{\theta}} = \tilde{\boldsymbol{H}}'^{-1}\tilde{\boldsymbol{P}} - \tilde{\boldsymbol{H}}'^{-1}\boldsymbol{N}\boldsymbol{L}^{-1}\tilde{\boldsymbol{Q}} \tag{30}$$

$$\tilde{\boldsymbol{V}} = \tilde{\boldsymbol{L}}'^{-1}\tilde{\boldsymbol{Q}} - \tilde{\boldsymbol{L}}'^{-1}\boldsymbol{M}\boldsymbol{H}^{-1}\tilde{\boldsymbol{P}} \tag{31}$$

The approximation always holds for a radial system or a meshed system with a constant r/x ratio, as justified by the theoretical derivation presented in this section. For more complex cases, the approximation error is mild, as can be demonstrated by a numerical example.

A. An Illustrative Example

Let us begin with a 2-bus system (see Fig. 3) for illustration. In this case, equation (13) becomes

$$\begin{bmatrix} \boldsymbol{H} & \boldsymbol{N} \\ \boldsymbol{M} & \boldsymbol{L} \end{bmatrix} = \begin{bmatrix} -b_{12} & g_{12} \\ -g_{12} & -b_{12}-b_{22} \end{bmatrix} \tag{32}$$

and $\tilde{\boldsymbol{H}}$ and $\tilde{\boldsymbol{L}}$ can be calculated as follows:

$$\begin{aligned} \tilde{\boldsymbol{H}} &= \boldsymbol{H} - \boldsymbol{N}\boldsymbol{L}^{-1}\boldsymbol{M} \\ &= -b_{12} - g_{12}(b_{12}+b_{22})^{-1}g_{12} \\ &\approx -b_{12} - g_{12}b_{12}^{-1}g_{12} \\ &= \frac{1}{x_{12}} \end{aligned} \tag{33}$$

$$\begin{aligned} \tilde{\boldsymbol{L}} &= \boldsymbol{L} - \boldsymbol{M}\boldsymbol{H}^{-1}\boldsymbol{N} \\ &= -b_{12} - b_{22} - g_{12}b_{12}^{-1}g_{12} \\ &= \frac{1}{x_{12}} + \frac{1}{x_{22}} \end{aligned} \tag{34}$$

It can be seen from (33) and (34) that the updated elements are exactly identical to the diagonal elements of $\tilde{\boldsymbol{H}}'$ and $\tilde{\boldsymbol{L}}'$. This surprising feature can be extended to more general cases, as demonstrated next.

B. Theoretical Derivation

For a general power system, $\tilde{\boldsymbol{H}}$ and $\tilde{\boldsymbol{L}}$ are too complicated to explicitly derive. However, for a radial system or a constant-r/x-ratio system without PV buses, it can be proven that $\tilde{\boldsymbol{L}}'$ is identical to $\tilde{\boldsymbol{L}}$, whereas $\tilde{\boldsymbol{H}}'$ is a good approximation of $\tilde{\boldsymbol{H}}$.

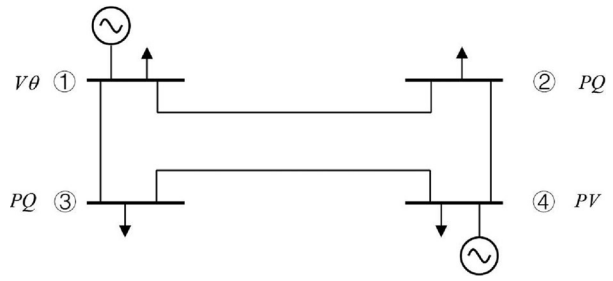

Fig. 4. Grainger & Stevenson 4-bus system.

Let $\boldsymbol{y}_{sc} = \boldsymbol{g}_{sc} + j\boldsymbol{b}_{sc}$ denote the primitive admittance matrix of a system in which the $V\theta$ buses are grounded and all shunt susceptances are neglected. $\boldsymbol{C}$ represents the node-to-branch incidence matrix. The shunt susceptances are represented by the $(n-1)\times(n-1)$ diagonal matrix $\boldsymbol{diag}\,(b_0)$.

For a meshed system with a constant r/x ratio, let us assume that for any branch l, $r_l/x_l = \alpha$. This leads to

$$g_l = -\frac{r_l}{x_l}\frac{-x_l}{r_l^2+x_l^2} = -\alpha b_l$$

$$\left(1+\alpha^2\right) b_l = \left(1+\frac{r_l^2}{x_l^2}\right)\frac{-x_l}{r_l^2+x_l^2} = -\frac{1}{x_l} \tag{35}$$

and thus

$$\begin{aligned}
\tilde{\boldsymbol{H}} &= \boldsymbol{H} - \boldsymbol{N}\boldsymbol{L}^{-1}\boldsymbol{M} \\
&= -\boldsymbol{C}\boldsymbol{b}_{sc}\boldsymbol{C}^T - \left(\boldsymbol{C}\boldsymbol{g}_{sc}\boldsymbol{C}^T\right) \\
&\quad \cdot \left(\boldsymbol{C}\boldsymbol{b}_{sc}\boldsymbol{C}^T + \boldsymbol{diag}\,(b_0)\right)^{-1}\left(\boldsymbol{C}\boldsymbol{g}_{sc}\boldsymbol{C}^T\right) \\
&\approx -\boldsymbol{C}\boldsymbol{b}_{sc}\boldsymbol{C}^T - \alpha^2\left(\boldsymbol{C}\boldsymbol{b}_{sc}\boldsymbol{C}^T\right) \\
&\quad \cdot \left(\boldsymbol{C}\boldsymbol{b}_{sc}\boldsymbol{C}^T\right)^{-1}\left(\boldsymbol{C}\boldsymbol{b}_{sc}\boldsymbol{C}^T\right) \\
&= -\left(1+\alpha^2\right)\boldsymbol{C}\boldsymbol{b}_{sc}\boldsymbol{C}^T \\
&= \tilde{\boldsymbol{H}}'
\end{aligned} \tag{36}$$

$$\begin{aligned}
\tilde{\boldsymbol{L}} &= \boldsymbol{L} - \boldsymbol{M}\boldsymbol{H}^{-1}\boldsymbol{N} \\
&= -\boldsymbol{C}\boldsymbol{b}_{sc}\boldsymbol{C}^T - \boldsymbol{diag}\,(b_0) \\
&\quad - \left(\boldsymbol{C}\boldsymbol{g}_{sc}\boldsymbol{C}^T\right)\left(\boldsymbol{C}\boldsymbol{b}_{sc}\boldsymbol{C}^T\right)^{-1}\left(\boldsymbol{C}\boldsymbol{g}_{sc}\boldsymbol{C}^T\right) \\
&= -\left(1+\alpha^2\right)\boldsymbol{C}\boldsymbol{b}_{sc}\boldsymbol{C}^T - \boldsymbol{diag}\,(b_0) \\
&= \tilde{\boldsymbol{L}}'
\end{aligned} \tag{37}$$

For a radial system (usually a distribution system), $\boldsymbol{C}$ is a non-singular matrix. It can also be easily found that $\tilde{\boldsymbol{L}}' = \tilde{\boldsymbol{L}}$ and $\tilde{\boldsymbol{H}}' \approx \tilde{\boldsymbol{H}}$, in the same manner as for meshed systems.

C. A Numerical Example

The approximations of $\tilde{\boldsymbol{H}}$ and $\tilde{\boldsymbol{L}}$ also hold for more general meshed systems. Let us demonstrate this claim using a numerical example of a Grainger & Stevenson 4-bus system [14], which is shown in Fig. 4.

Using equation (13), the matrices $\boldsymbol{H}$, $\boldsymbol{N}$, $\boldsymbol{M}$, and $\boldsymbol{L}$ are as follows:

$$\begin{bmatrix} \boldsymbol{H} & \boldsymbol{N} \\ \boldsymbol{M} & \boldsymbol{L} \end{bmatrix} = \left[\begin{array}{ccc|cc} 40.97 & -25.85 & -15.12 & -5.17 & -3.02 \\ -25.85 & 44.93 & 0 & 8.99 & 0 \\ -15.12 & 0 & 40.97 & 0 & 8.19 \\ \hline 5.17 & -8.99 & 0 & 44.84 & 0 \\ 3.02 & 0 & -8.19 & 0 & 40.86 \end{array}\right]$$

The matrices $\tilde{\boldsymbol{H}}$ and $\tilde{\boldsymbol{L}}$ are derived from equation (18) and (19):

$$\tilde{\boldsymbol{H}} = \begin{bmatrix} 41.79 & -26.88 & -15.72 \\ -26.88 & 46.73 & 0 \\ -15.72 & 0 & 42.61 \end{bmatrix}, \tilde{\boldsymbol{L}} = \begin{bmatrix} 46.63 & 0 \\ 0 & 42.50 \end{bmatrix}$$

The approximate matrices $\tilde{\boldsymbol{H}}'$ and $\tilde{\boldsymbol{L}}'$ are defined by (28) and (29):

$$\tilde{\boldsymbol{H}}' = \begin{bmatrix} 42.60 & -26.88 & -15.72 \\ -26.88 & 46.72 & 0 \\ -15.72 & 0 & 42.61 \end{bmatrix}, \tilde{\boldsymbol{L}}' = \begin{bmatrix} 46.63 & 0 \\ 0 & 42.50 \end{bmatrix}$$

It can be easily seen that $\tilde{\boldsymbol{L}}'$ and $\tilde{\boldsymbol{L}}$ are identical, whereas $\tilde{\boldsymbol{H}}'$ is extremely close to $\tilde{\boldsymbol{H}}$.

IV. Steps and Computational Complexity of the FDLPF Model

Many equations and demonstrations are presented in the sections above. To avoid confusion, this section summarizes and highlights the essential equations of the FDLPF model to be used for direct power flow calculations or related applications. For optimization problems, the proposed DLPF model (8) can be used directly, but this topic is outside the scope of this paper.

The following steps should be applied for the computation of bus voltage magnitudes and phase angles as well as the branch MW flows. The computational complexity is explained for each step.

1) *Step 1 Create matrices*

Create the admittance matrices $\boldsymbol{Y}$ and $\boldsymbol{Y}'$ and generate $\boldsymbol{H}$, $\boldsymbol{N}$, $\boldsymbol{M}$, and $\boldsymbol{L}$ at the PQ and PV buses according to (13). Create the matrices $\tilde{\boldsymbol{H}}'$ and $\tilde{\boldsymbol{L}}'$ using definitions (28) and (29).

Computational Complexity: All matrices are created directly from the system topology.

2) *Step 2 Modify bus power injections*

Build the modified bus injection vectors $\tilde{\boldsymbol{P}}$ and $\tilde{\boldsymbol{Q}}$ according to (12). Calculate $\boldsymbol{L}^{-1}\tilde{\boldsymbol{Q}}$ and $\boldsymbol{H}^{-1}\tilde{\boldsymbol{P}}$ first, followed by $\tilde{\boldsymbol{P}} - \boldsymbol{N}\boldsymbol{L}^{-1}\tilde{\boldsymbol{Q}}$ and $\tilde{\boldsymbol{Q}} - \boldsymbol{M}\boldsymbol{H}^{-1}\tilde{\boldsymbol{P}}$.

Computational Complexity: This step requires the factorization of two sparse matrices, $\boldsymbol{H}$ and $\boldsymbol{L}$.

3) *Step 3 Calculate bus voltage magnitudes, phase angles and MW flows*

The phase angles and voltage magnitudes can be rapidly calculated using expressions (30) and (31). The branch MW flows can be calculated using expression (7).

Computational Complexity: This step requires the factorization of two sparse matrices, $\tilde{\boldsymbol{H}}'$ and $\tilde{\boldsymbol{L}}'$.

TABLE I
ERRORS OF DIFFERENT LINEAR POWER FLOW MODELS FOR DISTRIBUTION SYSTEMS

Test Case	$\varepsilon_V^{DCPF\dagger}$	$\varepsilon_V^{md-[12]}$	$\varepsilon_V^{md-[11]}$	ε_V^{DLPF}	ε_V^{FDLPF}	ε_P^{DCPF}	$\varepsilon_P^{md-[12]}$	$\varepsilon_P^{md-[11]\ddagger}$	ε_P^{DLPF}	ε_P^{FDLPF}
IEEE 33-node	0.052	0.027	0.004	0.004	0.004	0.026	0.847	0.979	0.026	0.026
IEEE 123-node	0.051	0.027	0.004	0.003	0.003	0.008	0.291	0.173	0.008	0.008

†The bus voltage profile is assumed to be flat at 1.0 p.u. in the DCPF model.
‡The linear expression for branch MW flow is not provided in [11]. Because the phase angle is accurate, according to the results reported in [11], we assume the same expression as that for the DCPF model, namely, $\forall$ branches (i,j), $P_{(i,j)} = (\theta_i - \theta_j)/x_{ij}$.

The total computational complexity is very low for the following three reasons:

1) All of the matrices are created directly from the system topology. Because all of the matrices have the same structure as that of the admittance matrix, they can be updated rapidly after system reconfiguration.
2) All of the matrices are sparse and easily factorized.
3) All of the multiplication is performed between a matrix and a vector.

In the next section, it is shown that the FDLPF model is as fast as the classical DC power flow model.

V. NUMERICAL STUDIES

In this section, several cases are analyzed to demonstrate the accuracy and robustness of the DLPF/FDLPF approach and the fast computation speed of the FDLPF model [15]. Various types of power systems are studied:

1) Balanced radial distribution systems, including the IEEE 33-node test feeder [16] and the modified 123-node test feeder [11]. These systems are characterized by a radial topology and a high r/x ratio [17]. Because voltage drop is an important phenomenon in distribution systems [18], [19], these cases are studied to demonstrate the accuracy of the DLPF/FDLPF approach in terms of voltage magnitude.
2) Meshed transmission systems, including IEEE standard systems, large-scale Polish systems and Pegase systems. Most of the available cases are tested to demonstrate the robustness of the DLPF/FDLPF approach. The computation times for large-scale systems are also compared to illustrate the fast speed of the FDLPF model and the usefulness of the proposed approximation.
3) Ill-conditioned systems, which can be readily simulated by increasing the demand within the IEEE 33-node test feeder. This study is presented to demonstrate the ability of the DLPF/FDLPF approach to cope with an ill-conditioned system on the brink of collapse.

The analyses were performed in MATLAB with the aid of MATPOWER 5.1 [20]. The simulation platform was a ThinkPad workstation with an Intel i7 CPU@2.60 GHz and 8 GB of RAM. Three important results were obtained for comparison: bus voltage magnitudes, branch MW flows and computation times. With the results of the AC power flow model as the benchmark, the error for each model (md) was calculated as follows:

$$\varepsilon_V^{md} = \frac{1}{n}\sum_{i=1}^{n}\left|V_i^{md} - V_i^{AC}\right| \quad \text{(p.u.)} \tag{38}$$

$$\varepsilon_P^{md} = \frac{1}{m}\sum_{i=1}^{m}\left|P_i^{md} - P_i^{AC}\right| \quad \text{(p.u.)} \tag{39}$$

To avoid random timing errors, each MATLAB program was run ten times and the average computation time t^{md} was considered.

A. Balanced Radial Distribution Systems

Table I compares the performances of different models on the IEEE 33- and 123-node test feeders. The solutions were obtained using the DC power flow (DCPF) model, the method proposed in [12] (md-[12]), the method proposed in [11] (md-[11]) and the DLPF/FDLPF approach proposed in this paper. Fig. 5 visualizes the solutions for the 33-node system in terms of voltage magnitudes and branch MW flows. It should be noted that an average error of 0.05 p.u. in voltage magnitude is beyond tolerance, given that the operational voltage limit is typically between 0.95 p.u. and 1.05 p.u.

From Table I and Fig. 5, it is obvious that the DLPF and the FDLPF model perform the best not only in voltage magnitudes but in active power flows as well. Note that md-[11] exhibits the same accuracy in bus voltage magnitudes as the DLPF/FDLPF model but a poor performance in branch MW flows. This is not due to the flaws in the model itself but our choice to use DCPF branch flow expression, as no linear expression for branch MW flow is provided in [11]. In fact, the proposed model is a generalization of md-[11] from radial distribution systems to meshed networks with PV buses. A detailed discussion is provided in the Appendix.

B. Meshed Transmission Systems

Table II compares the performances of the different models for various kinds of transmission systems. The model proposed in [11] is excluded from this comparison because it was designed only for radial networks. Fig. 6 visualizes the solutions for the IEEE 118-bus system in terms of voltage magnitude and branch MW flow as an example for illustration. A comparison of the computation times for the large-scale system is also presented in Table III.

From Table II and Fig. 6, it is evident that the results of the DLPF and FDLPF models are the most accurate in terms of

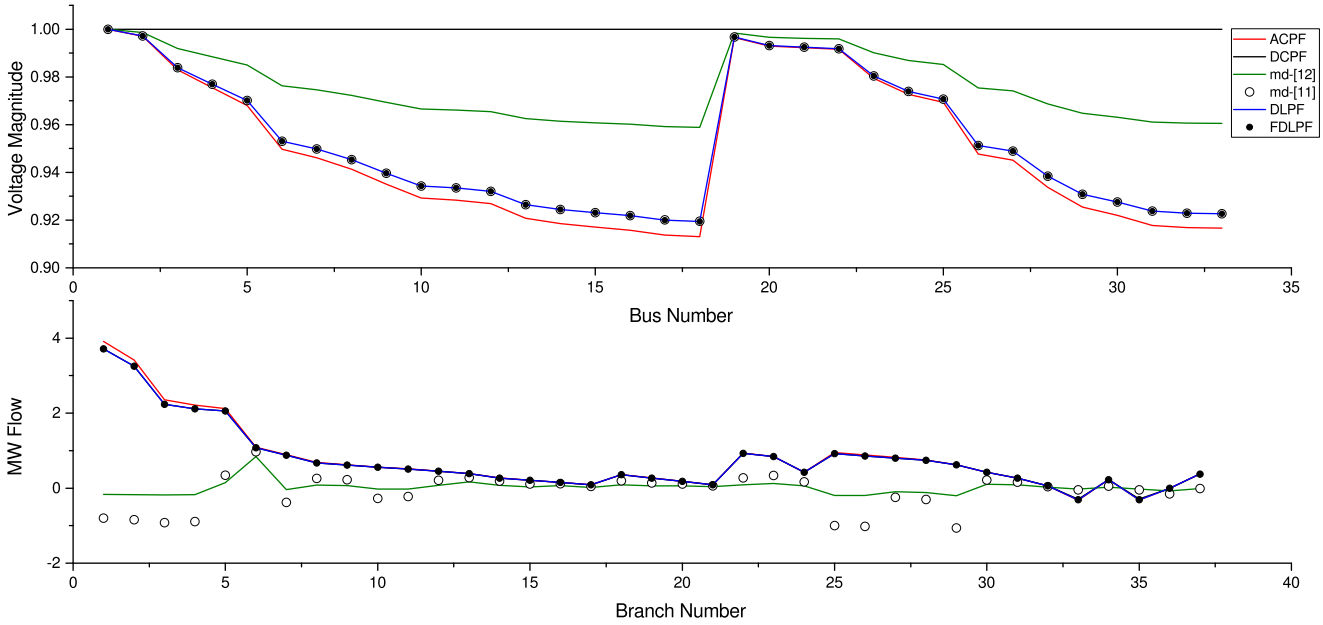

Fig. 5. Voltage magnitudes and branch MW flows for the IEEE 33-node test feeder.

TABLE II
ERRORS OF DIFFERENT LINEAR POWER FLOW MODELS FOR TRANSMISSION SYSTEMS

Test Case	$\varepsilon_V^{DCPF\dagger}$	$\varepsilon_V^{md-[12]}$	ε_V^{DLPF}	ε_V^{FDLPF}	ε_P^{DCPF}	$\varepsilon_P^{md-[12]}$	ε_P^{DLPF}	ε_P^{FDLPF}
IEEE 30-bus	0.018	0.011	0.001	0.001	0.004	0.023	0.002	0.007
IEEE 57-bus	0.024	0.012	0.007	0.009	0.015	0.062	0.010	0.017
IEEE 118-bus	0.023	0.003	0.001	0.001	0.035	0.090	0.034	0.042
IEEE 300-bus	0.025	0.016	0.014	0.014	0.105	0.148	0.102	0.105
Polish 2383-bus	0.008	0.005	0.003	0.003	0.026	0.047	0.022	0.038
Polish 3012-bus	0.089	0.005	0.002	0.003	0.022	0.055	0.021	0.034
Pegase 2869-bus	0.034	0.008	0.008	0.008	0.119	0.157	0.115	0.119
Pegase 9241-bus	0.032	0.014	0.007	0.007	0.181	0.208	0.178	0.192

†The bus voltage profile is assumed to be flat at 1.0 p.u. in the DCPF model.

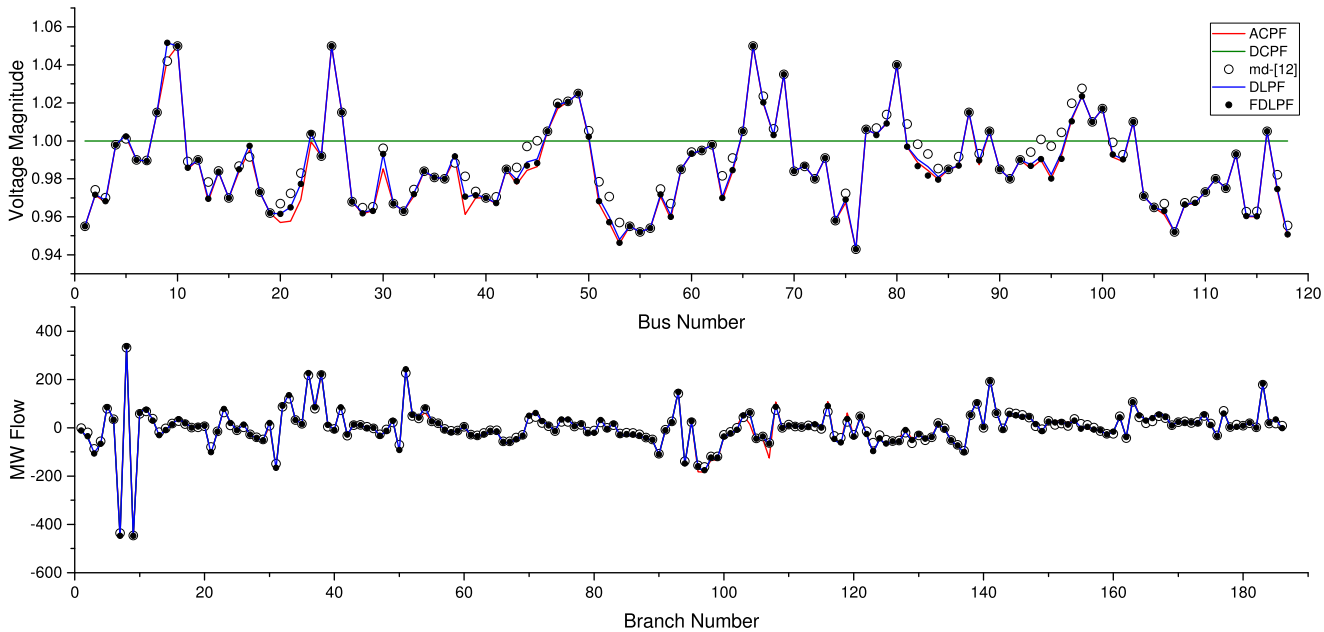

Fig. 6. Voltage magnitudes and branch MW flows for the IEEE 118-bus system.

TABLE III
COMPUTATIONAL EFFICIENCIES OF DIFFERENT LINEAR POWER FLOW MODELS FOR LARGE-SCALE SYSTEMS

Test Case	t^{ACPF} †	t^{DCPF}	$t^{md-[12]}$	t^{DLPF}	t^{FDLPF}
Polish 2383	0.24	0.01	1.75	1.60	0.01
Polish 3012	0.27	0.02	5.60	9.42	0.02
Pegase 2869	0.30	0.02	1.90	1.71	0.02
Pegase 9241	4.03	0.08	43.0	110	0.09

†The unit of computational time is second.

voltage magnitude among various cases of large-scale transmission systems. The accuracy of the DLPF model in terms of MW flow is also higher than that of the classical DC power flow model. Although the FDLPF model performs a little worse than the DC power flow model with respect of MW flow in some cases, the errors are acceptable because the main advantage of FDLPF is its accurate evaluation of bus voltage magnitudes. Moreover, Table III suggests that the FDLPF model achieves significantly improved computational efficiency by sacrificing only limited precision in terms of MW flow while maintaining the voltage magnitude accuracy of the DLPF model. The FDLPF model is therefore suitable for applications that require a large number of repeated load flow calculations.

A comparison of the computation times for the large-scale system is presented in Table III. Comparing it with Table II suggests that the FDLPF model achieves significantly improved computational efficiency by sacrificing only limited precision in terms of MW flow while maintaining the voltage magnitude accuracy of the DLPF model. The FDLPF model is therefore suitable for applications that require a large number of repeated load flow calculations.

C. Ill-Conditioned Systems

For the first considered case of an ill-conditioned system, the uniform overload of the system was simulated. The active and reactive demands on all buses were incrementally increased until the Newton-Raphson method was unable to converge. Similarly, for the second considered case, we increased the demand on a single bus (the 30th bus) to simulate a lumped overload scenario. Figs. 7 and 8 report the errors of the DLPF and FDLPF model in terms of voltage magnitude at different load levels. A comparison among the results of the different methods in the two cases shows that the DLPF and FDLPF models exhibit a performance not worse than the other linear power flow models for ill-conditioned systems.

VI. APPLICATION: SENSITIVITY FACTORS AND DISTRIBUTION SHIFT FACTORS

Using the fast and accurate FDLPF model proposed in this paper, the sensitivity factors for the bus voltage magnitudes and phase angles as well as the distribution shift factors for the branch MW flows can be easily determined with respect to nodal power injection. Notably, these factors can be applied in large-

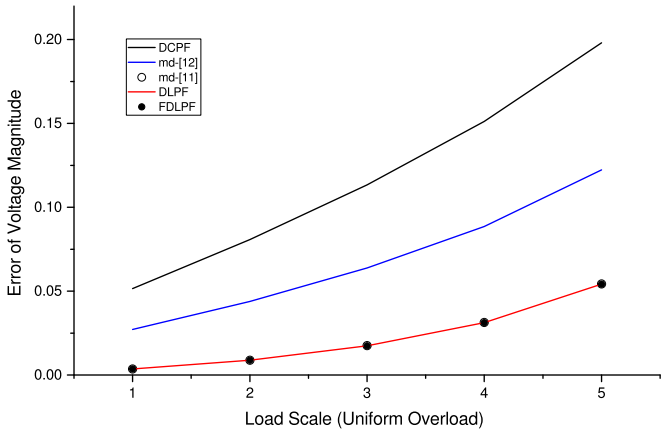

Fig. 7. 33-node ill-conditioned system (uniform overload).

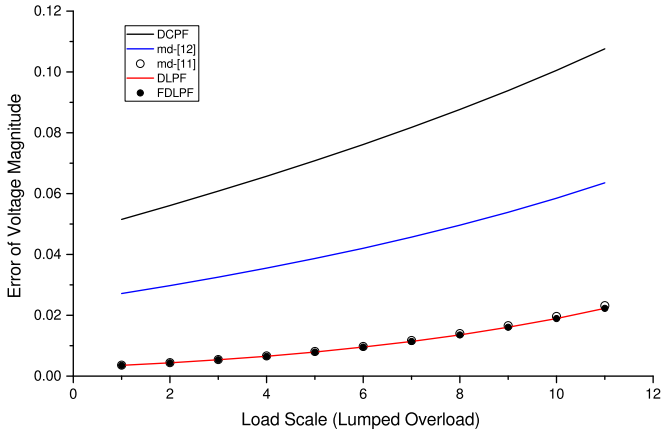

Fig. 8. 33-node ill-conditioned system (lumped overload).

signal cases because the FDLPF model is a state-independent cold-start model.

For simplicity and without loss of generality, we assume that the active and reactive power injections vary at a single bus i and that the perturbations are ΔP_i and ΔQ_i. According to expressions (30), (31) and (7), the corresponding changes in the voltage magnitude and phase angle at bus j are as follows:

$$\Delta\theta_j = \tilde{H}'^{-1}_{ji}\Delta P_i - \tilde{N}_{ji}\Delta Q_i \tag{40}$$

$$\Delta V_j = \tilde{L}'^{-1}_{ji}\Delta Q_i - \tilde{M}_{ji}\Delta P_i \tag{41}$$

where $\tilde{H}'^{-1}_{ji}$, $\tilde{L}'^{-1}_{ji}$, $\tilde{N}_{ji}$, and $\tilde{M}_{ji}$ denote the elements in the jth row and ith column of the matrices $\tilde{\boldsymbol{H}}'^{-1}$, $\tilde{\boldsymbol{L}}'^{-1}$, $\tilde{\boldsymbol{N}}$, and $\tilde{\boldsymbol{M}}$, respectively, where $\tilde{\boldsymbol{N}} = \tilde{\boldsymbol{H}}'^{-1}\boldsymbol{N}\boldsymbol{L}^{-1}$ and $\tilde{\boldsymbol{M}} = \tilde{\boldsymbol{L}}'^{-1}\boldsymbol{M}\boldsymbol{H}^{-1}$.

In the same manner, the distribution shift factor of a branch MW flow with respect to nodal power injection is as follows:

$$\begin{aligned}\Delta P_{(m,n)} &= g_{mn}\left(\Delta V_m - \Delta V_n\right) - b_{mn}\left(\Delta\theta_m - \Delta\theta_n\right)\\ &= \left(g_{mn}\left(\tilde{L}'^{-1}_{mi} - \tilde{L}'^{-1}_{ni}\right) + b_{mn}\left(\tilde{N}_{mi} - \tilde{N}_{ni}\right)\right)\Delta Q_i\\ &\quad - \left(b_{mn}\left(\tilde{H}'^{-1}_{mi} - \tilde{H}'^{-1}_{ni}\right)\right.\\ &\quad \left. + g_{mn}\left(\tilde{M}_{mi} - \tilde{M}_{ni}\right)\right)\Delta P_i\end{aligned} \tag{42}$$

TABLE IV
TEST OF THE SENSITIVITY FACTORS AND DISTRIBUTION SHIFT FACTORS DERIVED FROM THE FDLPF MODEL

Perturbation†	FDLPF SF	DCPF SF	Jacobian-based Voltage SF‡	With AC Power Flow
$\Delta\theta_2$	0.0292	0.0314	–	0.0303
$\Delta\theta_3$	0.0085	0.0085	–	0.0090
ΔV_2	0.0148	–	0.0113	0.0155
ΔV_3	0	–	0	−0.0002
$\Delta P_{(1,2)}$	−0.6125	−0.6226	–	−0.6297
$\Delta P_{(1,3)}$	−0.2186	−0.2274	–	−0.2235
$\Delta P_{(2,4)}$	0.2375	0.2274	–	0.2248
$\Delta P_{(3,4)}$	−0.2186	−0.2274	–	−0.2253

†$\Delta\theta$, ΔV, and ΔP are given in units of p.u.
‡SF is short for sensitivity factor. The Jacobian-based bus voltage sensitivity is given in [21].

Note that the matrices $\tilde{H}'^{-1}_{ji}$, $\tilde{L}'^{-1}_{ji}$, $\tilde{N}_{ji}$, and $\tilde{M}_{ji}$ are constant for a system with a fixed topology. They can also be rapidly updated after system reconfiguration because $\tilde{\boldsymbol{H}}'$, $\tilde{\boldsymbol{L}}'$, $\boldsymbol{N}$, and $\boldsymbol{M}$ have the same structure as that of the admittance matrix.

Table IV summarizes the sensitivity factors and distribution shift factors for the 4-bus system shown in Fig. 4. The changes in bus voltage, phase angle, and branch MW flow were calculated and compared with the results of the AC power flow model with P_2 and Q_2 reduced by 50% ($\Delta P_2 = 0.85$ p.u. and $\Delta Q_2 = 0.52$ p.u.). The results show that the proposed sensitivity factors perform with the highest accuracy in addressing the bus voltage. The phase angle and MW flow variations can also be calculated with reasonable accuracy.

An example of the calculation of the perturbation of the voltage magnitudes on all PQ buses in the 4-bus system is provided below:

$$\tilde{\boldsymbol{L}}'^{-1} = \begin{bmatrix} 0.0214 & 0 \\ 0 & 0.0235 \end{bmatrix}, \tilde{\boldsymbol{M}} = \begin{bmatrix} 0 & -0.0043 & 0 \\ 0 & 0 & -0.0047 \end{bmatrix}$$

$$\Delta V_2 = 0.0214 \times 0.52 + 0.0043 \times 0.85 = 0.0148$$

$$\Delta V_3 = 0 \times 0.52 - 0 \times 0.85 = 0$$

VII. CONCLUSION

In this paper, we propose a state-independent, $V-\theta$ DLPF model which is distinguished by high accuracy in voltage magnitude. An in-depth analysis of the matrices used for calculation is presented, giving rise to a fast version of the DLPF model, namely, the FDLPF model. The approximation that is applied to obtain the FDLPF model from the DLPF model is justified by a theoretical derivation and numerical examples. An analysis of various cases, including radial distribution systems with high r/x ratios, large-scale transmission systems and ill-conditioned systems, proves the accuracy and robustness of the two proposed power flow models. In large-scale cases, the FDLPF model is proven to be much faster than the DLPF model, thereby demonstrating the effectiveness of the approximation technique. Finally, the sensitivity factors and distribution shift factors are derived from the FDLPF model as a promising application.

We envision that the proposed models can serve as useful tools in power system planning and operation. Specifically, the DLPF model has the potential to be employed in optimization problem in place of the AC power flow equations, which may allow nonlinear, non-convex problems to be transformed into linear programming problems. In addition, the FDLPF model is characterized by high computational efficiency and has the potential to be applied in contingency analysis and probabilistic load flow problems. By utilizing the FDLPF model, voltage magnitude and reactive power can be considered as in the AC power flow model with a computational efficiency that is as high as that of the classical DC power flow model.

APPENDIX

Lemma 1: Let $\boldsymbol{Y}$ denote the admittance matrix of a radial distribution system, where there are typically no PV buses and the shunt admittances are negligible. Partition $\boldsymbol{Y}$ by the type of slack bus and PQ buses as follows:

$$\boldsymbol{Y} = \begin{bmatrix} \boldsymbol{Y}_{\mathcal{RR}} & \boldsymbol{Y}_{\mathcal{RL}} \\ \boldsymbol{Y}_{\mathcal{LR}} & \boldsymbol{Y}_{\mathcal{LL}} \end{bmatrix}$$

then

$$\boldsymbol{Y}_{\mathcal{LR}} = -\boldsymbol{Y}_{\mathcal{LL}} \cdot \mathbf{1}$$

where $\mathbf{1}$ is the vector of all ones.

Proof: As the shunt admittances are negligible, we have

$$\boldsymbol{Y} \cdot \mathbf{1} = \mathbf{0}$$

then

$$\boldsymbol{Y}_{\mathcal{LR}} + \boldsymbol{Y}_{\mathcal{LL}} \cdot \mathbf{1} = \mathbf{0}$$

Therefore,

$$\boldsymbol{Y}_{\mathcal{LR}} = -\boldsymbol{Y}_{\mathcal{LL}} \cdot \mathbf{1}$$

Lemma 2: For a complex matrix $\boldsymbol{C} = \boldsymbol{A} + j\boldsymbol{B}$ in which the $\boldsymbol{A}$ and $\boldsymbol{B}$ are nonsingular matrices, the inverse matrix of $\boldsymbol{C}$ is

$$\boldsymbol{C}^{-1} = \left(\boldsymbol{B} + \boldsymbol{A}\boldsymbol{B}^{-1}\boldsymbol{A}\right)^{-1}\boldsymbol{A}\boldsymbol{B}^{-1} - j\left(\boldsymbol{B} + \boldsymbol{A}\boldsymbol{B}^{-1}\boldsymbol{A}\right)^{-1}$$

Proof:

$$\begin{aligned} \boldsymbol{C}^{-1}\boldsymbol{C} = {} & \left(\boldsymbol{B} + \boldsymbol{A}\boldsymbol{B}^{-1}\boldsymbol{A}\right)^{-1}\boldsymbol{A}\boldsymbol{B}^{-1}\boldsymbol{A} \\ & + \left(\boldsymbol{B} + \boldsymbol{A}\boldsymbol{B}^{-1}\boldsymbol{A}\right)^{-1}\boldsymbol{B} \\ & + j\left(\boldsymbol{B} + \boldsymbol{A}\boldsymbol{B}^{-1}\boldsymbol{A}\right)^{-1}\boldsymbol{A}\boldsymbol{B}^{-1}\boldsymbol{B} \\ & - j\left(\boldsymbol{B} + \boldsymbol{A}\boldsymbol{B}^{-1}\boldsymbol{A}\right)^{-1}\boldsymbol{A} \\ = {} & \left(\boldsymbol{B} + \boldsymbol{A}\boldsymbol{B}^{-1}\boldsymbol{A}\right)^{-1}\left(\boldsymbol{B} + \boldsymbol{A}\boldsymbol{B}^{-1}\boldsymbol{A}\right) \\ = {} & \boldsymbol{I} \end{aligned}$$

Therefore, $\boldsymbol{C}^{-1}$ is the inverse matrix of $\boldsymbol{C}$. ■

For the method proposed in this paper, the bus voltage magnitudes are calculated using equation (21). $\boldsymbol{H}, \boldsymbol{N}, \boldsymbol{M}, \boldsymbol{L}$ in equation (21) are represented by

$$\begin{bmatrix} \boldsymbol{H} & \boldsymbol{N} \\ \boldsymbol{M} & \boldsymbol{L} \end{bmatrix} = -\begin{bmatrix} \boldsymbol{B}_{\mathcal{LL}} & -\boldsymbol{G}_{\mathcal{LL}} \\ \boldsymbol{G}_{\mathcal{LL}} & \boldsymbol{B}_{\mathcal{LL}} \end{bmatrix}$$

and

$$\tilde{\boldsymbol{L}} = -\left(\boldsymbol{B}_{\mathcal{LL}} + \boldsymbol{G}_{\mathcal{LL}}\boldsymbol{B}_{\mathcal{LL}}^{-1}\boldsymbol{G}_{\mathcal{LL}}\right)$$

According to (21) and *Lemma 1*, we have

$$\begin{aligned}\boldsymbol{V}_{\mathcal{L}} &= \tilde{\boldsymbol{L}}^{-1}\left(\boldsymbol{Q}_{\mathcal{L}} + \boldsymbol{B}_{\mathcal{LR}}V_0\right) - \tilde{\boldsymbol{L}}^{-1}\boldsymbol{G}_{\mathcal{LL}}\boldsymbol{B}_{\mathcal{LL}}^{-1}\left(\boldsymbol{P}_{\mathcal{L}} - \boldsymbol{G}_{\mathcal{LR}}V_0\right)\\ &= \tilde{\boldsymbol{L}}^{-1}\boldsymbol{Q}_{\mathcal{L}} - \tilde{\boldsymbol{L}}^{-1}\boldsymbol{G}_{\mathcal{LL}}\boldsymbol{B}_{\mathcal{LL}}^{-1}\boldsymbol{P}_{\mathcal{L}}\\ &\quad + \tilde{\boldsymbol{L}}^{-1}\left(\boldsymbol{B}_{\mathcal{LR}} + \boldsymbol{G}_{\mathcal{LL}}\boldsymbol{B}_{\mathcal{LL}}^{-1}\boldsymbol{G}_{\mathcal{LR}}\right)V_0\\ &= \tilde{\boldsymbol{L}}^{-1}\boldsymbol{Q}_{\mathcal{L}} - \tilde{\boldsymbol{L}}^{-1}\boldsymbol{G}_{\mathcal{LL}}\boldsymbol{B}_{\mathcal{LL}}^{-1}\boldsymbol{P}_{\mathcal{L}} + \tilde{\boldsymbol{L}}^{-1}\left(\tilde{\boldsymbol{L}}\cdot\boldsymbol{1}\right)V_0\\ &= \boldsymbol{1}V_0 + \tilde{\boldsymbol{L}}^{-1}\boldsymbol{Q}_{\mathcal{L}} - \tilde{\boldsymbol{L}}^{-1}\boldsymbol{G}_{\mathcal{LL}}\boldsymbol{B}_{\mathcal{LL}}^{-1}\boldsymbol{P}_{\mathcal{L}} \qquad \text{(A1)}\end{aligned}$$

where $V_0, \boldsymbol{V}_{\mathcal{L}}$ are the voltage magnitudes at slack bus and the remaining PQ buses.

As to the model in [11]. the expression for bus voltage magnitudes in the radial network is given as:

$$\boldsymbol{V}_{\mathcal{L}} = \boldsymbol{1}V_0 + \frac{1}{V_0}Re\left(\boldsymbol{Z}_{\mathcal{LL}}\overline{\boldsymbol{S}}_{\mathcal{L}}\right) \qquad \text{(A2)}$$

where $\boldsymbol{Z}_{\mathcal{LL}}$ is the inverse matrix of $\boldsymbol{Y}_{\mathcal{LL}}$. $\boldsymbol{S}_{\mathcal{L}}$ is the nodel complex power injection at PQ buses. $\overline{\boldsymbol{S}}_{\mathcal{L}}$ is the complex conjugate.

With the help of *Lemma 2*, equation (A2) can be transformed as follows:

$$\begin{aligned}\boldsymbol{V}_{\mathcal{L}} &= \boldsymbol{1}V_0 + \frac{1}{V_0}\,\mathrm{Re}\left(\left(\boldsymbol{G}_{\mathcal{LL}} + j\boldsymbol{B}_{\mathcal{LL}}\right)^{-1}\left(\boldsymbol{P}_{\mathcal{L}} - j\boldsymbol{Q}_{\mathcal{L}}\right)\right)\\ &= \boldsymbol{1}V_0 + \frac{1}{V_0}\left(-\tilde{\boldsymbol{L}}^{-1}\boldsymbol{G}_{\mathcal{LL}}\boldsymbol{B}_{\mathcal{LL}}^{-1}\boldsymbol{P}_{\mathcal{L}} + \tilde{\boldsymbol{L}}^{-1}\boldsymbol{Q}_{\mathcal{L}}\right) \qquad \text{(A3)}\end{aligned}$$

From the derivation above, it is easy to verify that the difference between (A1) and (A3) is tiny in radial distribution system. If the bus voltage magnitude is 1 p.u. at the slack bus of the radial network, then the two methods give identical results.

REFERENCES

[1] M. K. Enns, J. J. Quada, and B. Sackett, "Fast linear contingency analysis," *IEEE Trans. Power App. Syst.*, vol. PAS-101, no. 4, pp. 783–791, Apr. 1982.

[2] R. Billinton and R. N. Allan, *Reliability Evaluation of Engineering Systems*. New York, NY, USA: Springer, 1992.

[3] Z. Hu and X. Wang, "A probabilistic load flow method considering branch outages," *IEEE Trans. Power Syst.*, vol. 21, no. 2, pp. 507–514, May 2006.

[4] F. Dorfler and F. Bullo, "Novel insights into lossless ac and dc power flow," in *Proc. IEEE Power & Energy Soc. General Meeting*, Jul. 2013, pp. 1–5.

[5] F. Li and R. Bo, "DCOPF-based LMP simulation: Algorithm, comparison with ACOPF, and sensitivity," *IEEE Trans. Power Syst.*, vol. 22, no. 4, pp. 1475–1485, Nov. 2007.

[6] H. Zhang, G. T. Heydt, V. Vittal, and J. Quintero, "An improved network model for transmission expansion planning considering reactive power and network losses," *IEEE Trans. Power Syst.*, vol. 28, no. 3, pp. 3471–3479, Aug. 2013.

[7] B. Stott, J. Jardim, and O. Alsac, "DC power flow revisited," *IEEE Trans. Power Syst.*, vol. 24, no. 3, pp. 1290–1300, Aug. 2009.

[8] V. Sarkar and S. Khaparde, "A comprehensive assessment of the evolution of financial transmission rights," *IEEE Trans. Power Syst.*, vol. 23, no. 4, pp. 1783–1795, Nov. 2008.

[9] *PJM Training Materials*. [Online]. Available: http://pjm.com/

[10] A. Leite da Silva and V. Arienti, "Probabilistic load flow by a multilinear simulation algorithm," *Proc. IEE*, vol. 137, no. 4, pp. 276–282, Jul. 1990.

[11] S. Bolognani and S. Zampieri, "On the existence and linear approximation of the power flow solution in power distribution networks," *IEEE Trans. Power Syst.*, vol. 31, no. 1, pp. 163–172, Jan. 2016.

[12] S. Fatemi, S. Abedi, G. Gharehpetian, S. Hosseinian, and M. Abedi, "Introducing a novel dc power flow method with reactive power considerations," *IEEE Trans. Power Syst.*, vol. 30, no. 6, pp. 3012–3023, Nov. 2015.

[13] D. Van Hertem, J. Verboomen, K. Purchala, R. Belmans, and W. Kling, "Usefulness of dc power flow for active power flow analysis with flow controlling devices," in *Proc. 8th IEE Int. Conf. AC and DC Power Transm.*, Mar. 2006, pp. 58–62.

[14] J. J. Grainger and W. D. Stevenson, *Power Systems Analysis*. New York, NY, USA: McGraw-Hill, 1994.

[15] *Source Code for the Linear Power Flow Models, Github*. [Online]. Available: https://github.com/Jingwei-THU/linear-power-flow

[16] M. E. Baran and F. F. Wu, "Network reconfiguration in distribution systems for loss reduction and load balancing," *IEEE Trans. Power Del.*, vol. 4, no. 2, pp. 1401–1407, Apr. 1989.

[17] A. Ymeri, L. Dervishi, and A. Qorolli, "Impacts of distributed generation in energy losses and voltage drop in 10 kV line in the distribution system," in *Proc. IEEE Int. Energy Conf.*, 2014, pp. 1315–1319.

[18] J. Huang *et al.*, "A diagnostic method for distribution networks based on power supply safety standards," *Protection Control Modern Power Syst.*, vol. 1, no. 1, pp. 1–8, 2016.

[19] Z. Esau and D. Jayaweera, "Reliability assessment in active distribution networks with detailed effects of PV systems," *J. Modern Power Syst. Clean Energy*, vol. 2, no. 1, pp. 59–68, 2014.

[20] R. Zimmerman, C. Murillo-Sanchez, and R. Thomas, "Matpower: Steady-state operations, planning, and analysis tools for power systems research and education," *IEEE Trans. Power Syst.*, vol. 26, no. 1, pp. 12–19, Feb. 2011.

[21] P. S. Seshadri and A. D. Patton, "Bus voltage sensitivity: An instrument for pricing voltage control service," in *Proc. IEEE Power Eng. Soc. Summer Meeting*, 1999, vol. 2, pp. 703–707.

Jingwei Yang (S'15) received the B.S. degree from the Electrical Engineering Department, Tsinghua University, Beijing, China, in 2015, where he is currently working toward the Ph.D. degree.

His research interests include optimal power flow, renewable energy, and multiple energy system integration.

Ning Zhang (S'10–M'12) received both the B.S. and Ph.D. degrees from the Electrical Engineering Department, Tsinghua University, Beijing, China, in 2007 and 2012, respectively.

He is currently an Assistant Professor with Tsinghua University. His research interests include stochastic analysis and simulation of renewable energy, power system planning and scheduling with renewable energy, and multiple energy system integration.

Chongqing Kang (M'01–SM'07–F'17) received the Ph.D. degree from the Department of Electrical Engineering, Tsinghua University, Beijing, China, in 1997.

He is currently a Professor with Tsinghua University. His research interests include power system planning, power system operation, renewable energy, low carbon electricity technology, and load forecasting.

Qing Xia (M'01–SM'08) received the Ph.D. degree from the Department of Electrical Engineering, Tsinghua University, Beijing, China, in 1989.

He is currently a Professor with Tsinghua University. His research interests include electricity markets, generation scheduling optimization, and power system planning.